

A Subspace Approach to Timing Acquisition for Wavelet-Based Multirate Transmissions

†Chih-Ming Fu, ‡Wen-Liang Hwang and †Chung-Lin Huang

†Department of Electrical Engineering, National Tsing Hua University

‡Institute of Information Science, Academia Sinica, Taiwan

Abstract

We propose a subspace-based maximum-likelihood (ML) approach for acquiring the timing of wavelet-based multirate transmission systems. The S-curve analysis shows that our approach can correctly acquire the initial timing of a symbol from anywhere within a symbol-time interval at a cost of increasing jitter variance.

1 Introduction

A discussion of promising paradigms that exploit wavelet filter banks to achieve reliable multirate transmission over wireless fading, $\frac{1}{f}$, and severe intersymbol interference channels can be found in [1]. Clock synchronization is a fundamental function of a baseband transmission system, the task of which is to estimate a system's time epoch that is necessary in the demodulation process. An interesting nondata-aided (NDA) ML-based method (ML-NDA) for tracking a wavelet-based multirate system is proposed in [2]. However, it is shown in [3] that ML-NDA cannot be used for correct timing acquisition because it produces many spurious local maxima within a symbol-timing interval. Although the ambiguity issue may

be solved during acquisition with trial-and-errors, we propose a systematic approach to resolve the ambiguity. Instead of applying the ML-method directly to the received signal, as in [2], we apply it to the received signal after it is projected into the subspace spanned by the translated scaling functions. Our approach capitalizes on two advantages of the translated scaling functions. First, a translated scaling function is a smooth function that reduces noise variance; and second, it is orthogonal to the wavelets if the translation is an integer multiple of the symbol-timing interval. We evaluate our method’s stability, speed of acquisition, and jitter variance by using the traditional synchronization analysis techniques in [4]. The analysis shows that our approach can correctly locate the timing of the initial symbol of a symbol stream. However, our simulation results show that our approach has a higher jitter variances than that proposed in [2] for tracking the later symbols. Thus, a hybrid approach that uses our method for acquisition and the method in [2] for tracking is a good approach to acquire the correct clock synchronization for a wavelet-based multirate transmission system.

Using the subspace approach as the pre-processing method for symbol synchronization has been proposed in [5, 6]. This is similar to our method because it projects the received signal into a subspace before ML is applied. Nevertheless, there are some differences between the two methods. The primary goal in [5, 6] is to derive the optimal shape pulse, from which self-noise is absent, by using wavelets as pre-filters. Our primary goal, on the other hand, is to derive the correct symbol timing acquisition algorithm. The remainder of this manuscript is organized as follows. In Section 2, we provide an outline of our system and propose our subspace-based ML-based synchronizer. In Section 3, the performance of our proposed method is evaluated. Finally, in Section 4, we present our conclusions.

2 Scaling Function Subspace Acquisition Method

We begin with an outline of our system, after which we propose our subspace ML-NDA synchronization method. We assume that carrier frequency and phase are recovered exactly

prior to clock extraction, or that the transmission is baseband. Let $\psi(t)$ be an orthogonal real-valued wavelet, and $\psi_{m,n}(t)$ be a scaled and translated version of $\psi(t)$ with

$$\psi_{m,n}(t) = 2^{m/2}\psi\left(\frac{2^m}{T_0}t - n\right), \quad (1)$$

where the translation and scale index n , m respectively denote the n th symbol of the m th subband; and the signaling interval $T_0/2^m$ in the m th subband is related to the signaling interval T_0 in the slowest subband. A multirate waveform is defined as the superposition of M different signal components, each supporting a different data rate and occupying a different subband as follows:

$$s(t) = A \sum_{m=0}^{M-1} \sum_n d_{m,n} \psi_{m,n}(t), \quad (2)$$

where A is a positive amplitude factor; $d_{m,n} \in \{\pm 1\}$ are independent, identically distributed (i.i.d.) binary data symbols.

We can write the received waveform for the additive white Gaussian noise (AWGN) channel as

$$r(t) = s(t - \tau) + w(t), \quad (3)$$

where $s(t)$ is given in Eq. (2), $\tau \in [0, T_0)$ denotes the channel delay to be estimated by a receiver, and $w(t)$ is AWGN with two-sided power spectral density $\sigma_w^2 = 1/2N_0$.

We introduce an ML-NDA clock acquisition algorithm in which the ML-function is derived from the received signal, after it is projected into the space spanned by the translated scaling functions.

Our acquisition function is

$$F_\phi(\hat{\theta}) = \sum_q |f_q(\hat{\theta})|^2, \quad (4)$$

where $f_q(\hat{\theta})$ is the inner product between the received signal $r(t)$ and the translated scaling function $\phi_{0,q}(t - \hat{\tau})$. The application of the ML approach to obtain this function is presented

in Appendix 1. The timing point that maximizes the acquisition function can be acquired by seeking the zero of

$$F'_\phi(\hat{\theta}) = \sum_q f_q(\hat{\theta}) f'_q(\hat{\theta}). \quad (5)$$

In the above equation, $f_q(\hat{\theta})$ is derived by

$$\begin{aligned} f_q(\hat{\theta}) &= \frac{1}{T_0} \int_{T_{obs}} [s(t - \tau) + w(t)] \phi_{0,q}(t - \hat{\tau}) dt \\ &= \sum_m \sum_n Ad_{m,n} R_{m,n,0,q}(\hat{\theta}) + z_q(\hat{\tau}), \end{aligned} \quad (6)$$

while $f'_q(\hat{\theta})$ is derived by

$$f'_q(\hat{\theta}) = \sum_m \sum_n Ad_{m,n} R'_{m,n,0,q}(\hat{\theta}) + z'_q(\hat{\tau}), \quad (7)$$

where $R_{m,n,0,q}(\hat{\theta})$ and $R'_{m,n,0,q}(\hat{\theta}) \triangleq dR_{m,n,0,q}(\hat{\theta})/d\hat{\theta}$ are the respective responses between $\psi_{m,n}(t - \tau)$ and the filter $\phi_{0,q}(\hat{\tau} - t)$ and its derivative. In addition, $z_q(\hat{\tau})$ and $z'_q(\hat{\tau})$ are the respective responses of $w(t)$ to the filter and the derivative filter of $\phi_{0,q}(\hat{\tau} - t)$. The zero in Eq. (5) is usually obtained by means of a linear feedback loop where the error signal is generated. The error signal $e_s(k)$ of our synchronizer is

$$e_s(k) \triangleq f_k(\hat{\theta}_k) f'_k(\hat{\theta}_k). \quad (8)$$

The discrete-time loop operation, in terms of normalized timing errors, is governed by the conventional recursion

$$\hat{\theta}_{k+1} = \hat{\theta}_k - \gamma e_s(k), \quad (9)$$

where γ is the algorithm stepsize.

3 Performance Evaluation

The performance of our synchronizer in terms of mean acquisition time and jitter variance is derived and measured by simulation. We performed our simulations on three-subband wavelet modulated signals with the Meyer wavelet.

Mean Acquisition Time

The mean acquisition time is the average number of iterations required by the discrete-time feedback loop to achieve the equilibrium point. The S-curve [4] is usually used to evaluate the performance of an acquisition algorithm for a noise free signal, and is defined as

$$S(\hat{\theta}) \triangleq E[e_s(k)|\hat{\theta}_k = \hat{\theta}]. \quad (10)$$

By substituting Eqs. (6) and (7) into Eq. (8) and imposing the assumption that our data has an independent and equal probability and zero-mean for symbols so that

$$E\{d_{p,q}d_{m,n}\} = \begin{cases} 1 & \text{if } p = m, q = n, \\ 0 & \text{otherwise,} \end{cases} \quad (11)$$

we can derive the S-curve as a function of $\hat{\theta}$:

$$S(\hat{\theta}) = A^2 \sum_m \sum_n \left[R_{m,n,0,k}(\hat{\theta}) R'_{m,n,0,k}(\hat{\theta}) \right]. \quad (12)$$

Ignoring the recursion number k and letting $A = 1$ for simplicity, the S-curve of our acquisition algorithm is shown in Fig. 1. Our curve is accurate, since it has only one zero at $\hat{\theta} = 0$ within the timing interval T_0 . The S-curve is also stable so that, if we start at any point at $[0, T_0)$, our feedback loop system will eventually lead to the equivalent point at $\hat{\theta} = 0$. Using the Meyer wavelet, the S-curve can be approximated as

$$S(\hat{\theta}) = A^2 D_s \sin(2\pi\hat{\theta}), \quad (13)$$

where $D_s = 0.13462$. For the Daubechies 4th-order wavelet basis, we have $D_s = 0.3966$. Fig. 2 gives an example of how our method acquires the correct timing, while the ML-NDL may diverge during acquisition of the timing of a signal. In this simulation, γ is set so that the loop system parameter $B_L T_0$ is 10^{-4} , where $B_L T_0 \approx \frac{\gamma D_s}{4}$. B_L is referred to as the noise equivalent bandwidth of the loop. The derivation of the bandwidth B_L can be found in [4].

The simulation result, as shown in the left subfigure of Fig. 3, is the average number of iterations needed to acquire the right timing with errors smaller than $10^{-3}T_0$ for noise free signals. If we assume that the initial error $\hat{\theta}_0$ is uniformly in $[0, T_0)$, the average number of iterations to acquire the correct timing of noisy signals with different E_b/N_0 is given in the right subfigure of Fig. 3. The number of iterations increases non-linearly as E_b/N_0 decreases.

Steady-State Jitter Variance

The steady-state jitter variance measures the performance of a synchronizer around the equilibrium point $\hat{\theta} = 0$. This measurement has been thoroughly analyzed in [4]. Thus, we only demonstrate the performance by simulation. In our simulation, the jitter variance is calculated by measuring $\sigma_{\hat{\theta}}^2 = E\{\hat{\theta}^2\}$ as a function of E_b/N_0 , where E_b is the data symbol energy. Fig. 4 shows the simulation result of the normalized error deviation $\sigma_{\hat{\theta}}$ and compares it to the modified Crámer-Rao bound (MCRB). The MCRB for a wavelet-based multirate system has been derived in [2]. After numerically fitting the simulated curves, the normalized error deviation of our synchronizer can be approximated to $\sigma_{\hat{\theta}} \cong 1.2726 \frac{B_L T_0}{E_b/N_0}$. The main components of the jitter variance are the thermal noise and the self noise [4]. The existence of self-noise prevents the jitter variance from further decreasing, even with a large E_b/N_0 . This self-noise is removed by using the proposed subspace approach to pre-process the received signal. This can be seen in the top subfigure of Fig. 4; when E_b/N_0 increases, our jitter variance decreases. Note that our simulation result is consistent with those derived in [5, 6] in which the self-noise is removed when data is modulated by a scaling function, and the received signal is pre-filtered by a wavelet. As shown in the bottom subfigure of Fig. 4, although our approach resolves the ambiguity issue arising from the ML-NDA method and removes the self-noise in jitter variance, our jitter variance is larger than that of ML-NDA with small E_b/N_0 .

4 Conclusion

We show that the proposed subspace-based ML approach can resolve the ambiguity issue in timing acquisition that arises from the NDA-ML method. Our simulation shows that this approach is better than the NDA-ML method for eliminating self-noise at the cost of a higher jitter variance with smaller E_b/N_0 . Combining our approach for acquiring the initial symbol and NDA-ML for tracking the later symbols of a symbol bitstream is a good approach for acquiring the correct clock synchronization of a wavelet-based multirate transmission system.

References

- [1] G. Wornell, “Emerging applications of multirate signal processing and wavelets in digital communications,” *Proc. IEEE*, vol. 84, pp. 586–603, Apr. 1996.
- [2] M. Luise, M. Marselli, and R. Reggiannini, “Clock synchronization for wavelet-based multirate transmissions,” *IEEE Trans. on Commun.*, vol. 48, pp. 1047–1054, June 2000.
- [3] C. M. Fu, W. L. Hwang, and C. L. Huang, “Timing acquisition for wavelet-based multirate transmissions,” *IEEE Globecom.*, 2003.
- [4] U. Mengali and A. N. D’Andrea, *Synchronization Techniques for Digital Receivers*, Plenum press . New York and London, 1997.
- [5] F. Daneshgaran, M. Mondin, and F. Dovic, “Symbol synchronization using wavelets,” *Proc. IEEE MILCOM*, pp. 891–895, 1995.
- [6] F. Daneshgaran and M. Mondin, “Wavelet-based signal design for reduced jitter timing-recovery,” *IEEE Trans. on Commu.*, vol. 45, no. 12, pp. 1523–1526, 1997.
- [7] H. Meyr, M. Moeneclaey, and S. Fechtel, *Digital Communication Receivers*, Wiley Interscience, 1998.

Appendix 1

The coefficients obtained by projecting the received signal $r(t)$ to the $\hat{\tau}$ -translated scaling function, $\phi_{0,q}(t - \hat{\tau})$, are

$$f_q(\hat{\theta}) = \langle r(t), \phi_{0,q}(t - \hat{\tau}) \rangle = s_q(\hat{\theta}) + w_q(\hat{\tau}). \quad (14)$$

We use the notation $g^{\phi(\hat{\tau})}(t)$ for the projection of the signal $g(t)$ into the space spanned by $\{\phi_{0,q}(t - \hat{\tau}) | q \in Z\}$. Thus, we have

$$g^{\phi(\hat{\tau})}(t) = \sum_q \langle g(t), \phi_{0,q}(t - \hat{\tau}) \rangle \phi_{0,q}(t - \hat{\tau}). \quad (15)$$

Let \mathbf{r} be the column vector of $f_q(\hat{\theta})$, with $q = 1, \dots, Q$. Since $w_q(\hat{\tau})$ is a zero-mean white Gaussian noise, the joint conditional density function of $P(\mathbf{r}|\hat{\theta})$ can be expressed as

$$p(\mathbf{r}|\hat{\theta}) = \left(\frac{1}{\sqrt{\frac{2\pi}{T_0} \sigma_w}} \right)^Q \exp \left[-\frac{1}{2\sigma_w^2/T_0} \int_{T_{obs}} [r^{\phi(\hat{\tau})}(t) - s^{\phi(\hat{\tau})}(t - \tau)]^2 dt \right].$$

The likelihood of the above equation is composed of three terms. After neglecting the common constants in the exponents of each, they are, respectively:

$$\begin{aligned} L_1(\mathbf{r}|\hat{\theta}) &= \exp \left[-\int_{T_{obs}} |r^{\phi(\hat{\tau})}(t)|^2 dt \right], \\ L_2(\mathbf{r}|\hat{\theta}) &= \exp \left[2 \int_{T_{obs}} r^{\phi(\hat{\tau})}(t) s^{\phi(\hat{\tau})}(t - \tau) dt \right], \\ L_3(\mathbf{r}|\hat{\theta}) &= \exp \left[-\int_{T_{obs}} |s^{\phi(\hat{\tau})}(t - \tau)|^2 dt \right]. \end{aligned}$$

The log-likelihood of each term is then derived as follows:

1. The log-likelihood of L_1 is

$$L_1^l(\mathbf{r}|\hat{\theta}) = -\sum_{m,n} \langle r^{\phi(\hat{\tau})}(t), \psi_{m,n}(t - \tau) \rangle \langle \psi_{m,n}(t - \tau), r^{\phi(\hat{\tau})}(t) \rangle \quad (16)$$

$$= -\sum_{m,n} \langle r^{\phi(\hat{\tau})}(t), \psi_{m,n}^{\phi(\hat{\tau})}(t - \tau) \rangle \langle \psi_{m,n}^{\phi(\hat{\tau})}(t - \tau), r^{\phi(\hat{\tau})}(t) \rangle \quad (17)$$

$$= -\sum_{m,n} |y_{m,n}^{\phi(\hat{\tau})}|^2. \quad (18)$$

For the above derivation, the equivalents of Eqs. (16) and (17) are given below. By substituting $\psi_{m,n}^{\phi(\hat{\tau})}(t - \tau)$ and $r^{\phi(\hat{\tau})}(t)$ into Eq. (15) and the orthogonality of the translated scaling functions $\langle \phi_{p,q}(t - \hat{\tau}), \phi_{m,n}(t - \hat{\tau}) \rangle = \delta_{p,m} \delta_{q,n}$, we have

$$\begin{aligned} \langle r^{\phi(\hat{\tau})}(t), \psi_{m,n}^{\phi(\hat{\tau})}(t - \tau) \rangle &= \sum_{p,q} \langle r^{\phi(\hat{\tau})}(t), \phi_{p,q}(t - \hat{\tau}) \rangle \langle \psi_{m,n}(t - \tau), \phi_{p,q}(t - \hat{\tau}) \rangle \\ &= \langle r^{\phi(\hat{\tau})}(t), \psi_{m,n}(t - \tau) \rangle. \end{aligned}$$

2. If our data is i.i.d. with binary PAM and equal probability, then we have

$$P(\mathbf{d}) = \prod_{m,n} P(d_{m,n}) = \prod_{m,n} \left(\frac{1}{2} \delta(d_{m,n} - 1) + \frac{1}{2} \delta(d_{m,n} + 1) \right).$$

By averaging out the data on $L_2(\mathbf{r}|\hat{\theta})$, it yields

$$\begin{aligned} \bar{L}_2(\mathbf{r}|\hat{\theta}) &= \int_{\mathbf{d}} L_2(\mathbf{r}|\hat{\theta}) P(\mathbf{d}) d\mathbf{d} \\ &= \prod_{m,n} \cosh 2A y_{m,n}^{\phi(\hat{\tau})} \end{aligned}$$

Since $\ln \cosh x \approx \frac{1}{2}x^2$ for small x [7, 2], we have

$$\bar{L}_2^l(\mathbf{r}|\hat{\theta}) \approx 2A^2 \sum_{m,n} |y_{m,n}^{\phi(\hat{\tau})}|^2. \quad (19)$$

3. The log-likelihood of L_3 is

$$\begin{aligned} - \int_{T_{obs}} |s^{\phi(\hat{\tau})}(t - \tau)|^2 dt &= - \sum_q \langle s(t - \tau), \phi_{0,q}(t - \hat{\tau}) \rangle \langle \phi_{0,q}(t - \hat{\tau}), s(t - \tau) \rangle \\ &\approx - \sum_q \langle r(t), \phi_{0,q}(t - \hat{\tau}) \rangle \langle \phi_{0,q}(t - \hat{\tau}), r(t) \rangle \end{aligned} \quad (20)$$

$$= - \int_{T_{obs}} |r^{\phi(\hat{\tau})}(t)|^2 dt \quad (21)$$

$$= - \sum_{m,n} |y_{m,n}^{\phi(\hat{\tau})}|^2 \quad (22)$$

where the approximation in Eq. (20) resulting from $w(t)$ is a white Gaussian noise and $\phi(t - \hat{\tau})$ is a low-pass smooth function. Summing up Eqs.(18), (19), and (22) yields

$$2(A^2 - 1) \sum_{m,n} |y_{m,n}^{\phi(\hat{\tau})}|^2. \quad (23)$$

Also, According to Eqs. (20), (21), (22) and (14), it is easily shown that

$$\sum_{m,n} |y_{m,n}^{\phi(\hat{\tau})}|^2 = \sum_q |f_q(\hat{\theta})|^2. \quad (24)$$

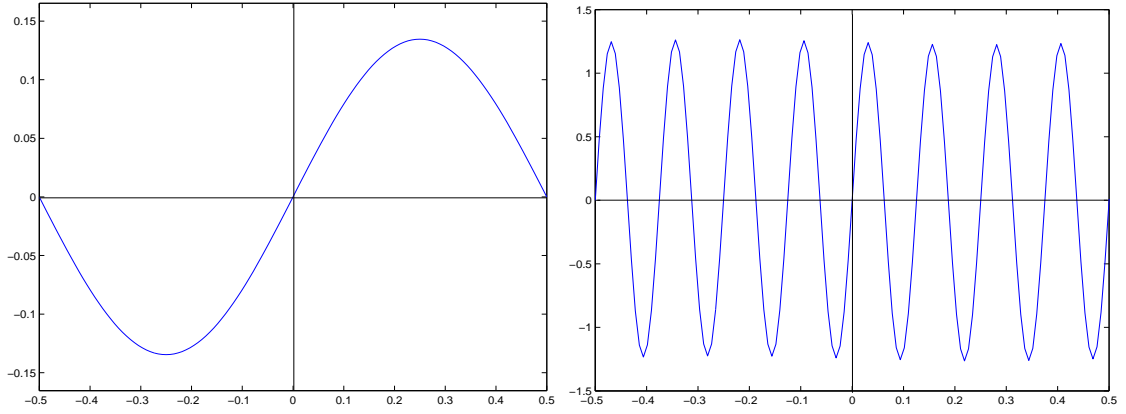


Figure 1: Comparison of the S-curve of the Meyer wavelet using different methods. Left: Our S-curve is stable, and there is only one zero crossing at the correct timing point within a normalized symbol interval, where the timing symbol is normalized to 1. Right: The S-curve of the ML-NDA method. There are many spurious local maxima within a normalized timing symbol interval.

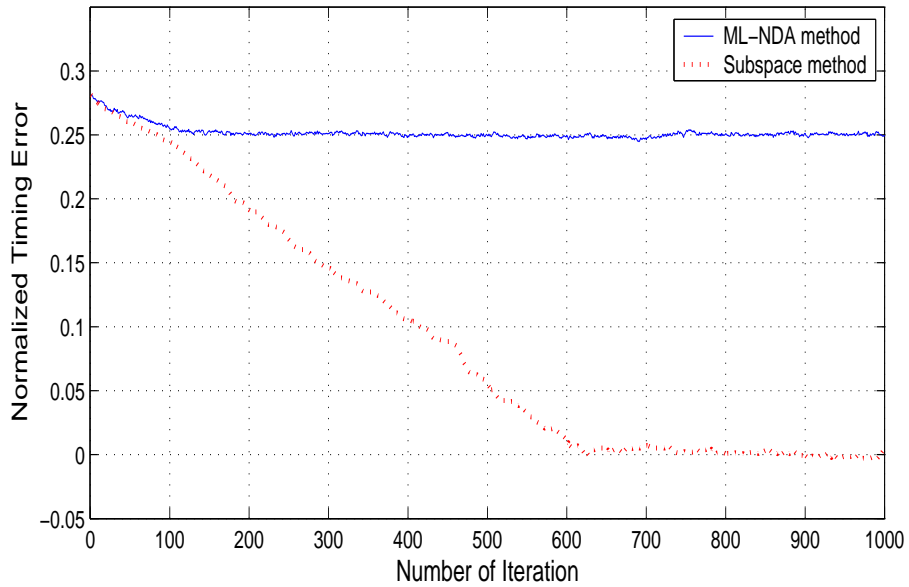


Figure 2: The regression of normalized clock error $\hat{\theta}$ and $e_s(k)$. The loop system parameter $B_L T_0$ is 10^{-4} . Unlike our curve, the ML-NDA curve does not converge to the correct timing point.

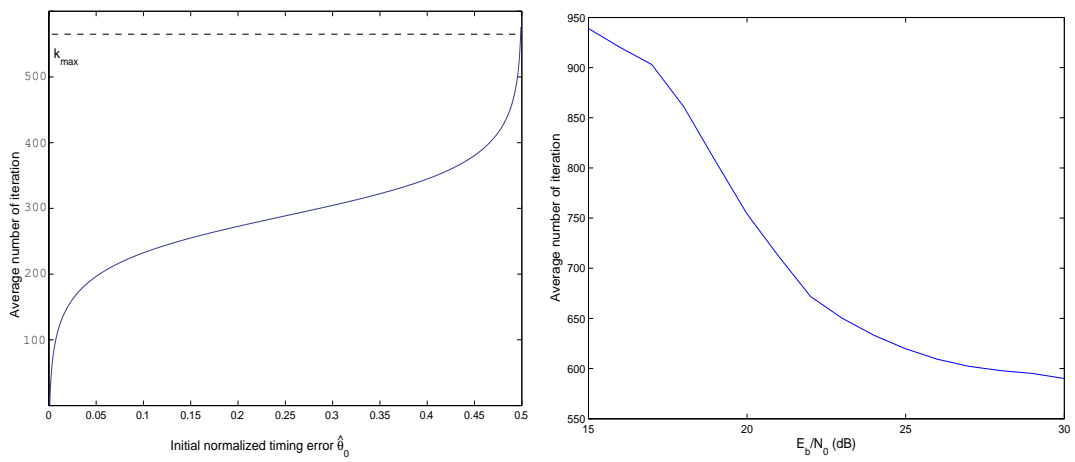


Figure 3: The average number of iterations to locate the correct timing by using our method. Left: Noise free signals, starting from a different initial error $\hat{\theta}_0$. Right: Noisy signals with different E_b/N_0 by assuming that $\hat{\theta}_0$ is uniformly distributed.

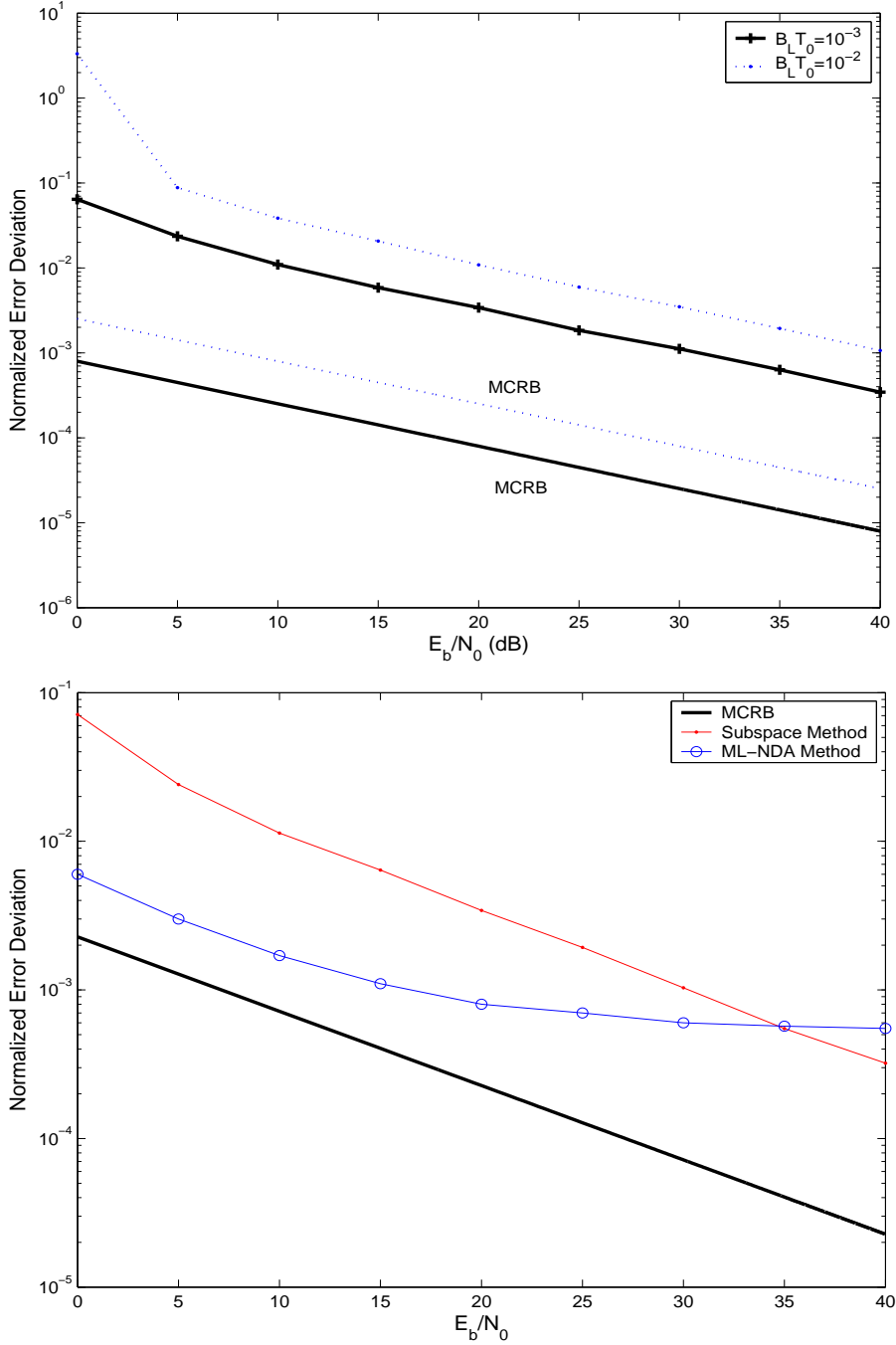


Figure 4: Normalized error deviation $\sigma_{\hat{\theta}}$ against E_b/N_0 . Top: The simulation was carried out on a three-subband clock synchronizer for two different sets of loop parameters. The bottom two curves are MCRB, derived by the formula in [2]. Bottom: Comparison of the jitter variance of our method with that of ML-NDA for a two-subband modulated signal with loop system parameter $B_L T_0 = 10^{-3}$.